2008

Experimental investigations of spontaneous bimaterial interfacial fractures

Kaiwen Xia

Carl-Ernst Rousseau
University of Rhode Island, roussce@uri.edu

Ares Rosakis

Citation/Publisher Attribution
Xia, K., Rousseau, C., & Rosakis, A. (2008). Experimental investigations of spontaneous bimaterial interfacial fractures. *Journal of Mechanics of Materials and Structures, 3*(1), 173-184. doi: 10.2140/jomms.2008.3.173
Available at: http://dx.doi.org/10.2140/jomms.2008.3.173

Experimental investigations of spontaneous bimaterial interfacial fractures

Journal of
Mechanics of
Materials and Structures

EXPERIMENTAL INVESTIGATIONS OF SPONTANEOUS BIMATERIAL INTERFACIAL FRACTURES

Kaiwen Xia, Carl-Ernst Rousseau and Ares Rosakis

Volume 3, Nº 1 January 2008

mathematical sciences publishers

JOURNAL OF MECHANICS OF MATERIALS AND STRUCTURES
Vol. 3, No. 1, 2008

EXPERIMENTAL INVESTIGATIONS OF SPONTANEOUS BIMATERIAL INTERFACIAL FRACTURES

KAIWEN XIA, CARL-ERNST ROUSSEAU AND ARES ROSAKIS

Following our innovative experimental spontaneous fracture models for frictional fractures (compression and shear) and mixed-mode fractures (tension and shear) in identical materials, we designed a laboratory model to investigate the effects of material contrast on mixed-mode spontaneous fracture along a bimaterial interface. A series of interesting phenomena are observed, including asymmetry of crack propagation, with different speeds and levels of fracture parameters. Crack tips fracture parameters are observed to depend on crack speeds, on far-field loading, and on far-field mode-mixity. A strong dependence is also identified between mode-mixity and crack length. Most importantly, the fracture parameters are found to exhibit a strong dependence upon crack length and only a weak dependence on crack speed as is commonly thought. These observations are discussed in details in relation to material contrast. It is expected that these observations will have a profound influence on engineering practice involving the application of materials and structures with bimaterial interfaces.

Introduction

Interfacial fracture has long been identified as one of the primary causes of failure in layered materials and adhesive joints, and has therefore received much scrutiny [Hutchinson and Suo 1992]. Interfacial fracture spans length scales from submicrons in multiphase nanomaterials to thousands of kilometers in geological faults. Among various scenarios, two situations can be commonly recognized under dominant tensile loading conditions [Kitey and Tippur 2005]. First, when an interface is stronger than the weaker constituent material, cracks tend to kink into the weak material and grow nearly parallel to the interface [Hutchinson et al. 1987]. Thus, failure is controlled by the properties of the weak material constituent. The second scenario appears when the interface is the weakest component in the bimaterial system, and crack initiation and propagation occurs along the interface. In the latter case, which will be elaborated upon in this paper, the weakness pertinent to such multimaterial systems arises from the inherent disadvantage present at interfaces that can be no stronger than the weaker of the two adjacent materials. The physical nature of such composites is further complicated by a discrepancy in elastic properties that gives rise to inbuilt mode-mixity in stress states.

Although the resulting cracks can initiate and propagate in either the quasistatic or the dynamic regime, the latter is more catastrophic and is also more difficult to evaluate experimentally and theoretically. Consequently, direct measurements of dynamic stress states for bimaterial cracks were initiated only a decade ago, utilizing optical methods combined with high speed photography. Pioneering experimental

Keywords: spontaneous dynamic fracture, bimaterial interfacial fracture, stress intensity factor, photoelasticity.
This work is partially supported by the University of Toronto through the start-up funding received by KX.

investigation in dynamic bimaterial fracture includes the works of Tippur and Rosakis [1991], Lambros and Rosakis [1995], and Singh and Shukla [1995].

Modeling of dynamic interfacial fracture, however, started earlier, dating back to the 1967 work by Goldshte [1967]. This work predicted the possibility of attaining wave speeds in excess of the lower of the two Rayleigh wave speeds of the material constituents. This was subsequently confirmed by Lambros and Rosakis [1995], by means of optical measurements. Several new experiments have since been conducted to further reinforce these findings.

Analytical developments have also emerged to assist in the interpretation of these experimental developments. Yang et al. [1991] have formulated expressions that describe the crack tip field for steadily growing interfacial cracks between two different isotropic materials. Through their work, the velocity dependence of the universal bimaterial oscillatory index was for the first time ascertained. Further, Deng [1993] performed a steady-state asymptotic analysis for interfacial cracks that resulted in the establishment of higher-order terms associated with the bimaterial crack tip stress field. Similar results for nonsteady-state crack growth soon followed. Indeed, Liu et al. [1993] uncovered the requisite analytical expressions along with the associated higher-order terms. The work was also accompanied by experimental investigation.

Although the historical context of this problem has focused on material decohesion, the associated concepts are applicable also to the modeling of earthquakes [Andrews and Ben-Zion 1997; Cochard and Rice 2000] and to the spontaneous rupture of unbonded but otherwise joined materials in relatively firm contact. The latter case, also called laboratory earthquakes, is intended to understand earthquakes resulting from disturbances to natural faults and was explored by Xia et al. [2005b]. Recently, the idea of spontaneous fracture experiments was extended to the study of coherent interfacial fractures between identical and dissimilar materials under far-field mixed-mode loading [Rosakis et al. 2006]. As will be discussed later, there are several advantages to using spontaneous experimental fracture setups over traditional interfacial experimental designs inherited from standard static fracture experiments such as three-point bent, compact tension, and wedge driving cracks. Another reason to investigate spontaneous fractures is that spontaneous fracture is the main dynamic crack failure mode in engineering materials and engineering structures. The present work expands upon the interfacial fracture under mixed-mode far-field loading [Rosakis et al. 2006] to establish a comprehensive and more complete understanding of dynamic interfacial failure in bimaterial systems.

Experimental design of spontaneous interfacial fracture

The bimaterial system consists of two adjoined birefringent materials, Homalite-100 and polycarbonate (9.5 mm in thickness), that exhibit different elastic and constitutive properties as shown in Table 1. The wave speeds listed in the table are measured using a 10 MHz ultrasonic sensor, while the remaining properties are obtained from the literature [Dally and Riley 1991]. The two equally sized plates are joined to form a complete square specimen with each side measuring 150 mm. Before bonding the two halves of the specimen, a small groove, 0.15 mm in depth, is machined on the interface of one of the two half plates through its thickness. A thin metal wire of diameter 0.1 mm is then placed in the groove and the plates are bonded using an adhesive with elastic properties similar to those of Homalite-100. However, the adhesive possesses a much lower fracture toughness than either of the base materials, which constrains

Material Property	Homalite-100	Polycarbonate
Young's Modulus E (MPa)	3860	2480
Poisson's Ratio ν	0.35	0.38
Stress fringe value f_σ (kN/m)	23.6	7.0
P Wave Speed C_P (km/s)	2.104	1.724
S Wave Speed C_S (km/s)	1.200	0.960
Density ρ (kg/m^3)	1230	1192

Table 1. Summary of optical and dynamic mechanical properties of photoelastic materials.

any possible propagating rupture to the interfacial corridor. An average interface thickness of 0.1 mm is achieved. The static mode-I fracture toughness of the bonding is 0.46 MPa-m$^{1/2}$ [Rosakis et al. 2006].

Figure 1 describes the configuration used in this study. The explosion box, which constitutes the most critical aspect of this experiment, provides the electric energy to transform the metal wire into a high pressure, high temperature plasma within 10 μs. The expansion of the plasma results in a controlled isotropic line loading pulse across the sample thickness [Xia et al. 2005a]. Upon ignition, the exploding wire creates a small incipient crack that propagates along the interface only because the toughness of the adhesive is lower than that of either of the constituents of the bimaterial system. If the far-field loading is large enough, this initial small crack is unstable and propagates dynamically.

The interface is inclined at an angle α to the horizontal direction. Therefore, the nature of the far-field loading provided through the uniaxial tension in the vertical direction is mixed-mode with respect to the fracture path (bonding line). Upon sending the ultra high electric voltage (several kilovolts) to the exploding wire, the explosion box simultaneously provides a low voltage level triggering signal to the high speed camera. The camera system (Cordin 220) is able to capture the images at a framing rate of 100 million frames per second with exposure times as low as 10 nanoseconds. In this specific study, the high speed camera is operated at a much slower speed, around 0.2–0.4 million frames per second. A uniquely designed tensile fixture is used to maintain a static far-field load in the vertical direction, which applies the load to the sample through two compressed springs by a hydraulic press. The sample is attached on two sides, top and bottom, to two steel plates, which are fixed to the loading fixture to apply different levels of tensile loading.

The spontaneous fracture setup has several advantages over traditional dynamic fracture experimental techniques. First, the flawless sample is loaded statically before the dynamic initiation and propagation of the fracture. This results in increased accuracy of the foreknowledge of the stress field. This is especially important for exacting stress intensity factors with the full-field optical diagnostics (photoelasticity in this study). Second, the load is time independent throughout the duration of the crack propagation. Thus, theoretically, the dynamic stress intensity factor is related to the equivalent static stress intensity factor through a universal function of crack speed [Yang et al. 1991; Freund 1990]. Third, the sudden initiation of the small incipient crack in the center of the specimen enables treatment of the problem, dynamically, as that of a finite crack extending in an infinite domain before the waves get reflected from the boundaries of the sample. This technique circumvents edge effects that are generally unavoidable in other designs

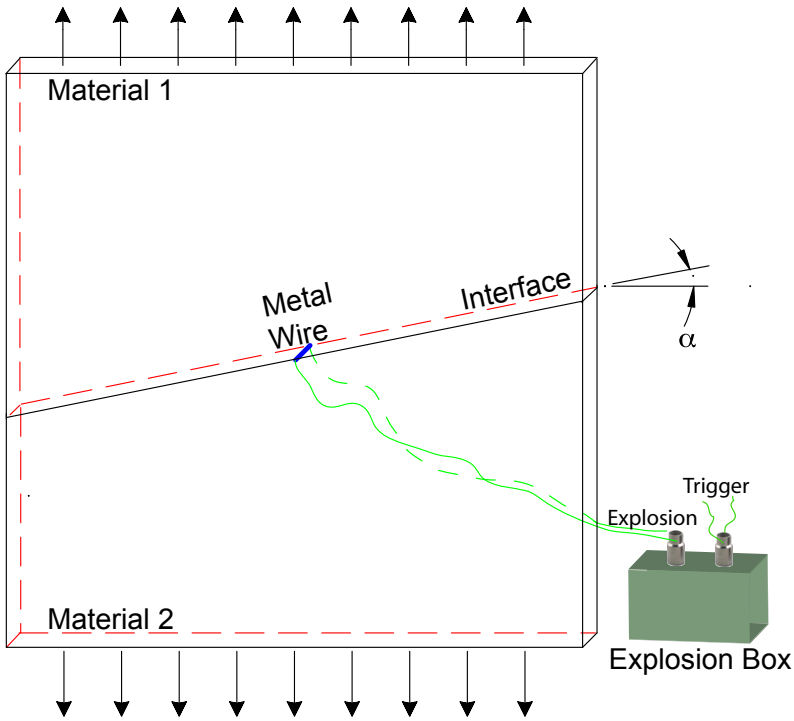

Figure 1. Specimen geometry of spontaneous fracture along bimaterial interface with the triggering mechanism.

of dynamic fracture experiments. Thus, existing exact analytical solutions may be used with confidence. Finally, the methodology used for initiating the crack provides an easy and reliable way to synchronize the diagnostic system (optical method combined with high speed photography) with the fracture process [Xia et al. 2004].

Extraction of stress intensity factor

A. Crack tip stress field at a bimaterial interface. Consider a crack propagating spontaneously and nonuniformly along a line defining the interface of two homogeneous, isotropic, and linearly elastic solids, at speeds bounded by the lowest Rayleigh wave speed pertaining to either material. The state of stress describing the ambient conditions surroundings such a two dimensional crack has been established by Liu et al. [1993], via asymptotic higher-order analysis. Relations necessary to the immediate and complete understanding of this experimental effort are reproduced below. Thus, individual stress components are given by:

$$\begin{aligned}
\sigma_{11}^{(m)} &= \mu\Re\left\{(1+2\alpha_l^2-\alpha_s^2)F_m''(z_l;t)+2\alpha_s G_m''(z_s;t)\right\},\\
\sigma_{22}^{(m)} &= -\mu\Re\left\{(1+\alpha_s^2)F_m''(z_l;t)+2\alpha_s G_m''(z_s;t)\right\},\\
\sigma_{12}^{(m)} &= -\mu\Im\left\{2\alpha_l F_m''(z_l;t)+(1+\alpha_s^2)G_m''(z_s;t)\right\}.
\end{aligned} \tag{1}$$

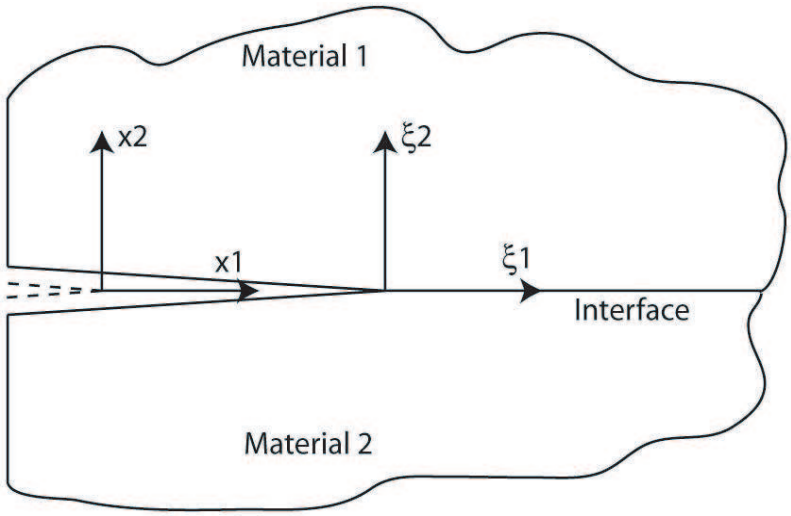

Figure 2. Schematic of dynamic growth of a crack along a bimaterial interface.

Each prime symbol denotes a derivative of the corresponding complex arguments, and $\Re$ and $\Im$ are the real and imaginary parts of the complex argument. The variable μ is the shear modulus of material 1 (see Figure 2).

Designating the longitudinal and shear wave speeds of the material by c_l and c_s, respectively, and the instantaneous crack speed by v, one can define the angle of inclination, α, as follows:

$$\alpha_{l,s}^2(t) = 1 - \frac{v^2(t)}{c_{l,s}^2}. \tag{2}$$

Further, a modified coordinate system is introduced such that $z_{l,s} = \eta_1 + i\alpha_{l,s}\eta_2$, where $\eta_i = (\xi_i/\varepsilon')$ and $i \in \{1, 2\}$, with ε' is a small arbitrary positive number. The complex functions $F(z_l; t)$ and $G(z_s; t)$ are defined as follows:

$$F_m(z_l;t) = -\frac{[(1+\alpha_s^2) - 2\eta\alpha_s]e^{\pi\varepsilon}}{\mu D(v)\cosh(\varepsilon\pi)} z_l^{3/2+i\varepsilon} A_m(z_l;t) + \frac{[(1+\alpha_s^2) + 2\eta\alpha_s]e^{-\pi\varepsilon}}{\mu D(v)\cosh(\varepsilon\pi)} z_l^{3/2-i\varepsilon}\overline{A}_m(z_l;t)$$
$$- \frac{1}{\mu D(v)}\left\{\left(\frac{1+\alpha_s^2}{1+\omega_l} - \frac{2\alpha_s}{1+\omega_s}\right)B_m(z_l;t) - \left(\frac{1+\alpha_s^2}{1+\omega_l} + \frac{2\alpha_s}{1+\omega_s}\right)\overline{B}_m(z_l;t)\right\} z_l^2, \tag{3}$$

and

$$G_m(z_s;t) = \frac{[2\alpha_l - \eta(1+\alpha_s^2)]e^{\pi\varepsilon}}{\mu D(v)\cosh(\varepsilon\pi)} z_s^{3/2+i\varepsilon} A_m(z_s;t) + \frac{[2\alpha_l + \eta(1+\alpha_s^2)]e^{-\pi\varepsilon}}{\mu D(v)\cosh(\varepsilon\pi)} z_s^{3/2-i\varepsilon}\overline{A}_m(z_s;t)$$
$$+ \frac{1}{\mu D(v)}\left\{\left(\frac{2\alpha_l}{1+\omega_l} - \frac{1+\alpha_s^2}{1+\omega_s}\right)B_m(z_s;t) - \left(\frac{2\alpha_l}{1+\omega_l} - \frac{1+\alpha_s^2}{1+\omega_s}\right)\overline{B}_m(z_l;t)\right\} z_s^2. \tag{4}$$

In the above equations, several new variables are introduced. However, they are all universal to the field of linear elastic fracture mechanics and their complete definition can be found in [Liu et al. 1993]

and in [Freund 1990]. $A_m(z,t)$ and $B_m(z,t)$ are entire function to be expanded into Taylor series, such that:

$$\begin{aligned} A_m(z,t) &= \sum_{n=0}^{\infty} A_m^{(n)}(t) z^n, \\ B_m(z,t) &= \sum_{n=0}^{\infty} B_m^{(n)}(t) z^n. \end{aligned} \tag{5}$$

In the present work, only the terms for which $m = 0$ are used in the expansions. In this case, the dynamic stress intensity factor is readily derived from the complex expression:

$$A_0^{(0)}(t) = -\frac{1}{2\sqrt{2\pi}} \frac{K^d(t)}{(3/2 + i\varepsilon)(1/2 + i\varepsilon)}. \tag{6}$$

Evaluation of the energy release rate follows directly from the stress intensity factor:

$$G = \frac{K_1^2 + K_2^2}{[4\cosh(\varepsilon\pi)]^2} \left[\left\{ \frac{\alpha_l(1-\alpha_s^2)}{\mu D(v)} \right\}_1 + \left\{ \frac{\alpha_l(1-\alpha_s^2)}{\mu D(v)} \right\}_2 \right], \tag{7}$$

where K_1 and K_2 are the real and imaginary arguments, respectively, of the complex bimaterial stress intensity factor. Finally, the mode-mixity inherent to all bimaterial systems is derived from the arctangent of the ratio of the imaginary to the real arguments of the stress intensity factor, or:

$$\psi = \tan^{-1}\left(\frac{K_2}{K_1}\right). \tag{8}$$

B. Extraction of fracture parameters. The fundamental relation pertaining to photoelasticity is represented by the stress-optic law:

$$\frac{N f_\sigma}{2h} = \tau_{\max}, \tag{9}$$

where N is the observed fringe order number, f_σ is the fringe constant of the photoelastic material, and h is the material thickness. The relation between these various parameters results in a visual representation of the contours of constant maximum shear stress in the material. Substitution of the dynamic bimaterial stress field equations into the above expression relates the isochromatic fringe patterns surrounding the advancing crack tip to dynamic stress intensity factor, crack tip speed, and other nonsingular higher-order terms, through:

$$\begin{aligned} \left(\frac{N f_\sigma}{2h}\right)^2 = \mu^2 \Big\{ &\left[(1+\alpha_l^2) \Re F_0''(z_l;t) + 2\alpha_s \Re G_0''(z_s;t) \right]^2 \\ &+ \left[2\alpha_l \Im F_0''(z_l;t) + (1+\alpha_s^2) \Im G_0''(z_s;t) \right]^2 \Big\}. \end{aligned} \tag{10}$$

In the present work inference of the dynamic stress intensity factor is conducted through an over deterministic method in which up to six higher-order terms are used. The unknown coefficients A_m and B_m appear as nonlinear terms in Equation (10). The solution is obtained by first designating the real and imaginary expressions of the above equation as D and T respectively. Subsequently, for each digitized

fringe data point, the following relation is established:

$$g_k = D_k^2 + T_k^2 - \left(\frac{N_k f_\sigma}{2h}\right)^2 = 0. \tag{11}$$

The set of k nonlinear equations is solved simultaneously using a least-squares analysis based on initial estimates of A_m and B_m. Correction factors are subsequently introduced, and the process is iterated until Equation (11) is satisfied to within an error upper bound of 0.0001. Further comprehensive details of the solution scheme can be found in the original work of Sanford and Dally [1979].

Experimental results and discussions

Experiments featuring spontaneous interfacial fractures between polycarbonate and Homalite-100, which were bonded along their common interface, were conducted. Each specimen possessed a different angle of inclination, α, and was loaded at a different level of uniaxial tension. The results of these experiments revealed that each specimen responded identically to the loading environment. First, the bilaterally propagating spontaneous fracture occurs at two different speeds. Second, shortly following fracture initiation, a constant speed level is established in both directions, with negligible variation. Finally, larger far-field load levels induce faster crack propagation.

A. Asymmetry of crack speeds and the variations of energy release rate. Figure 3 shows three typical isochromatic fringe patterns displayed with accompanying plots that identify crack-tip location and energy release rate histories featuring the different levels of uniaxial tension (7.5 MPa in (a) and (b), and 5.6 MPa in (c)). In Figures 3a and 3c, the inclination angle is 27.5°, while in Figure 3b, the inclination angle is 17.5°. Within each frame, the appearance of each set of fringes associated with each of the moving faults is clearly asymmetric. For instance the fringes coupled with the left moving cracks in the first two figures are larger than those pertaining to the right moving ones. This indicated greater stress levels, and therefore higher values of crack parameters. Also striking is the higher level of distortion pertaining to the right moving cracks in those same frames, a fact generally attributed to crack speeds approaching limiting values of the materials. The inverse is true for the third figure in the sequence.

Other observations can be drawn from these figures. First, the two crack tips propagate essentially at constant speeds with one end faster than the other. If the particle motion is resolved to coincide with the direction of the interface, propagation of the faster side is in the direction of the resolved shear particle motion of the more compliant constituent of the bimaterial system (polycarbonate). For the cases corresponding to Figures 3a and 3b, the lower material is more compliant, resulting in faster propagation to the right. In Figure 3c, the upper material is more compliant, causing the velocity trend to reverse. This asymmetry in speed is attributed to the existence of material contrast across the interface and the coupling between shear and tension resulting from this contrast [Cochard and Rice 2000; Weertman 1980]. For the case of shear fractures in frictionally held interfaces with combined shear and compressive loading, a configuration very different from the one tested here, similar phenomena have been predicted theoretically [Qian and Sun 1998] and have been observed experimentally [Xia et al. 2005b]. The shear induced compression may result in frictional contact of crack surfaces in both static and dynamic interfacial cracks in bimaterials [Sun and Qian 1997; Rosakis et al. 1998]. In the cases discussed here, however, the presence of the tensile load prevents any frictional contact behind the crack tip from interfering with crack

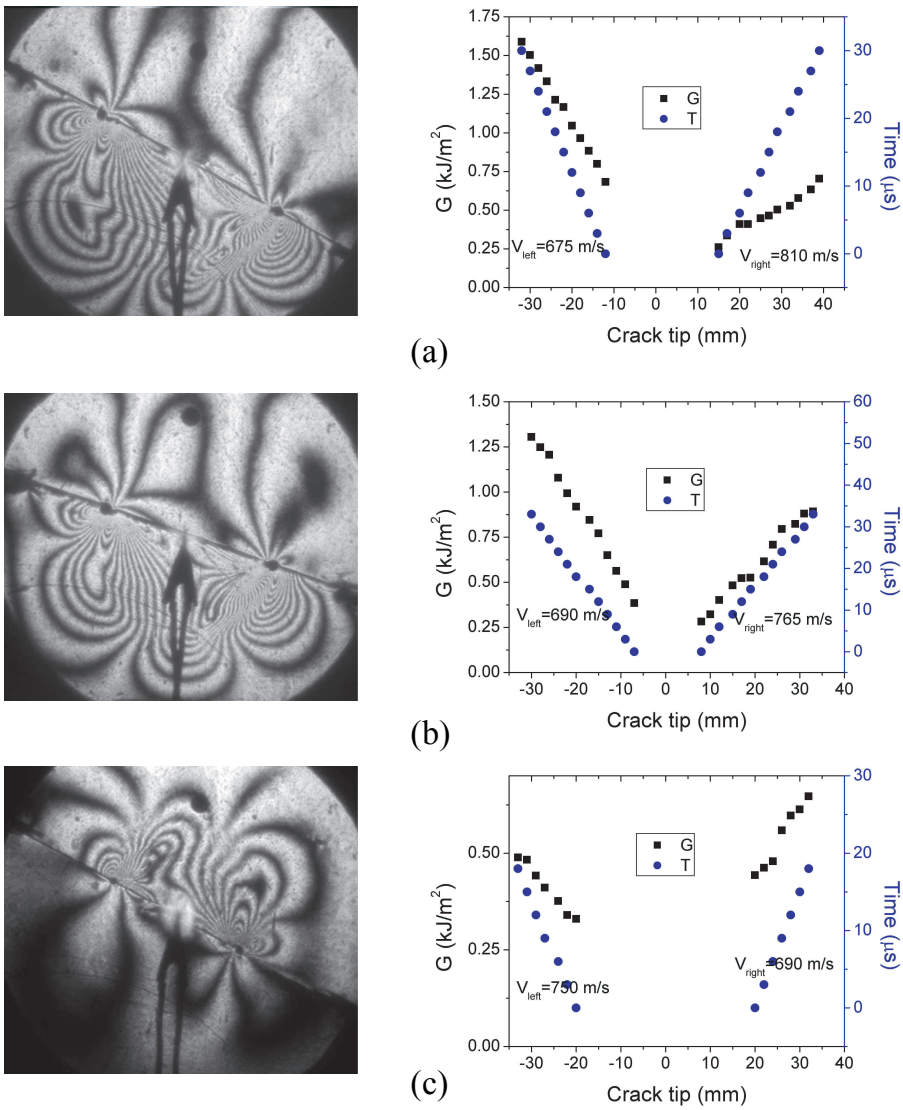

Figure 3. Isochromatic fringe patterns with plots of energy release rate and crack tip time history (The black dot on the top plate of each isochromatic picture is a 6.25 mm diameter length scale.). (a) Inclination angle is 27.5°, top is Homalite-100. (b) Inclination angle is 17.5°, top is Homalite-100. (c) Inclination angle is 27.5°, top is polycarbonate.

propagation. Indeed, from the isochromatic fringe patterns shown in Figure 3, no evidence of contact like those observed in stress wave induced dynamic shear crack propagation in bimaterial interfaces [Rosakis et al. 1998] can be identified. The observations here of asymmetric crack propagation further validate the theory of material contrast induced coupling between shear and normal motions.

It is noted that fracture energy, and equivalently energy release rate, increases linearly with the crack length at both crack locations. The fracture parameters are calculated using Equation (7), with stress intensity factors obtained by using the inversion scheme discussed above. A similar phenomenon, directly relating larger fracture parameters to increasing crack length, has also been identified for spontaneous mode I [Xia et al. 2006] and mixed-mode interfacial fracture in identically bonded materials [Rosakis et al. 2006]. As is the case for these earlier results, this increase of fracture energy with crack length is consistent with the observation of constant crack speeds and time independent loading, which implies that the dynamic energy release rate is related to the equivalent static energy release rate through the multiplication of a universal function depending only on the fracture velocity [Yang et al. 1991]. Consequently, for a given speed of spontaneous fracture, the energy release rate is proportional to the square of the equivalent static stress intensity factor. Since the equivalent static stress intensity factor is proportional to the square root of the crack length, the energy release rate is then proportional to the crack length. If, instead, the fracture energy remains constant during the crack propagation, the crack will accelerate to its limiting speed at which the energy release rate tends to zero and most of the released strain energy will be converted into kinetic energy [Freund 1990; Broberg 1999]. This observation of a constant speed crack thus casts doubt on the validity of using the fracture energy concept as a material parameter to describe crack propagation resistance. Crack propagation resistance, or, more precisely, the nominal crack propagation resistance that may involve damage of the crack path, might be more appropriately attributed to loading conditions and geometry [Broberg 2002]. It should also be noted that at the slower propagating end, the energy release rate is always larger than that of the faster end for the same length crack. This can be explained by the decreasing nature of the universal function dependence on the crack speed [Yang et al. 1991; Freund 1990; Broberg 1999].

B. Stress intensity factors and variations of mode-mixity. Figure 4 presents the crack tip history, energy release rate, stress intensity factors (K_1 for mode I and K_2 for mode II), and the mode-mixity ($\psi = \tan^{-1}(K_2/K_1)$ as in Equation (8)) for an experiment featuring 7.5 MPa far-field loading and 27.5° inclination angle. This test was performed under identical conditions as the one shown in Figure 3a.

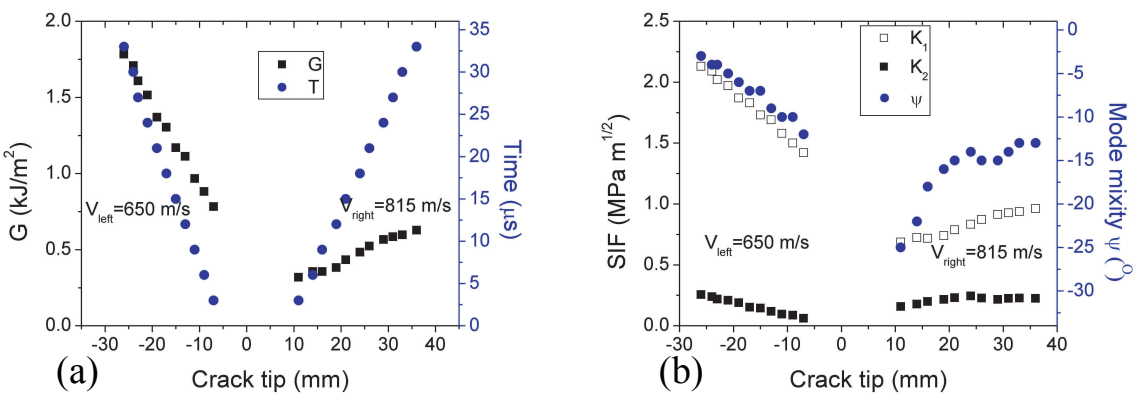

Figure 4. (a) Energy release rate (G), crack tip time history (T) and (b) the evolution of stress intensity factors (K_1, K_2) and mode-mixity (ψ) for a typical experiment.

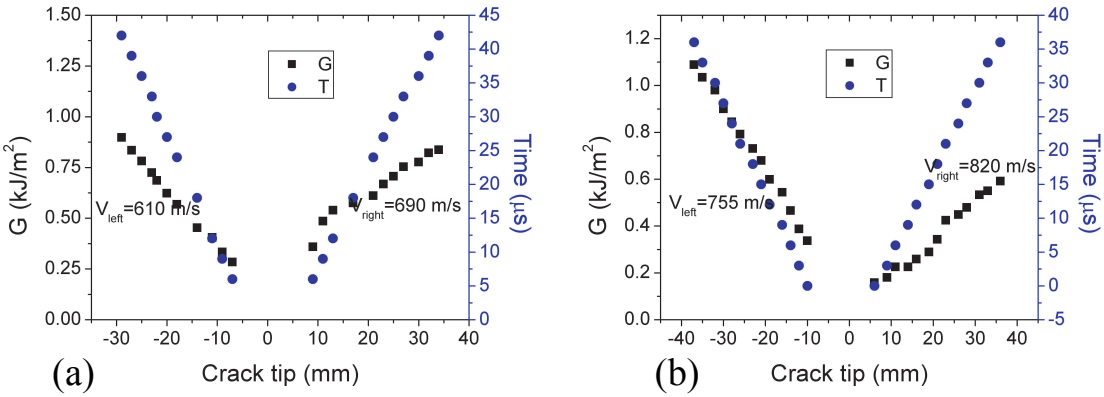

Figure 5. Figure 5. Energy release rate and crack tip time history. (a) Inclination angle is 25° and far-field load is 6.8 MPa. (b) Inclination angle is 25° and far-field load is 7.5 MPa.

Note that the crack speeds of the two experiments are very similar (Figure 4a), which demonstrates the repeatability of the experimental design.

As shown in Figure 4b, the mode-mixities of both ends are smaller than the far-field mode-mixity of 27.5°. The mode-mixity of the slower end is smaller than that of the faster end for the same length of propagation. The asymmetry is a result of the mode coupling discussed earlier. The fast crack tip has more mode II component than the slow crack tip. This result is consistent with that reported in the numerical simulation study of mixed-mode interfacial fracture propagation in identical materials [Geubelle and Kubair 2001]. The result is to be expected because the limiting speed of mode II cracks (longitudinal wave speed) is higher than that of mode I cracks (Rayleigh wave speed) [Freund 1990; Broberg 1999]. From a material response point of view, the result demonstrates that the debonding process is facilitated by greater prominence of mode II stress components. In other words, it is easier for a mixed-mode crack to propagate at fast speeds when it has higher levels of mode II components.

C. Dependence of crack speeds on far-field load. Figure 5 presents the crack tip history and energy release rate for two experiments featuring the same inclination angle (25°) and different load levels (7.5 MPa and 6.8 MPa respectively). Again it can be seen clearly that for both tests the energy release rate increases with the crack length. In the case where the load level is higher (Figure 5b), the speed of the left crack is faster than that corresponding to the case where the load level is lower (Figure 5a). The same conclusion holds for the right propagating crack. Detailed analytical study is needed to obtain the dependence of the crack speeds on far-field load. For self-similar mode I cracks, a theoretical relationship was proposed by Broberg [2002].

Conclusions

The experiments conducted herein feature bimaterial systems composed of polycarbonate and Homalite-100, bonded along an interface. Symmetric and central spontaneous initiation of a dual crack through plasma explosion resulted in asymmetric propagation, with the faster side proceeding in the direction of

the resolved shear particle motion of the more compliant constituent. This is the first published set of experiments where two opposing propagating cracks have been set to propagate simultaneously along a bimaterial interface. It is noted that the magnitude of the fracture parameters are always correlated to crack length. Surprisingly also, energy release rate is shown to be more weakly dependent on the crack speed than to the crack length, an observation that will undoubtedly stimulate theoretical discussions on the subject of crack propagation in general, and more specifically on crack propagation in bimaterial systems. It is also observed that higher load results in faster crack propagation.

Acknowledgements

Helpful discussions with Prof. G. Ravichandran from California Institute of Technology, with Prof. A. Shukla from University of Rhode Island, and with Prof. H. Gao from Brown University are acknowledged. The authors appreciate constructive comments from one anonymous reviewer.

References

[Andrews and Ben-Zion 1997] D. J. Andrews and Y. Ben-Zion, "Wrinkle-like slip pulse on a fault between different materials", *J. Geophys. Res.-Solid Earth* **102**:B1 (1997), 553–571.

[Broberg 1999] K. B. Broberg, *Cracks and fracture*, Academic Press., San Diego, 1999. 752.

[Broberg 2002] K. B. Broberg, "Constant velocity crack propagation - dependence on remote load", *Int. J. Solids Struct.* **39**:26 (2002), 6403–6410.

[Cochard and Rice 2000] A. Cochard and J. R. Rice, "Fault rupture between dissimilar materials: Ill-posedness, regularization, and slip-pulse response", *J. Geophys. Res.-Solid Earth* **105**:B11 (2000), 25891–25907.

[Dally and Riley 1991] J. W. Dally and W. F. Riley, *Experimental stress analysis*, 3rd ed. ed., McGraw-Hill, Inc., New York, 1991. 639.

[Deng 1993] X. Deng, "General crack-tip fields for stationary and steadily growing interface cracks in anisotropic bimaterials", *J. Appl. Mech. (Trans. ASME)* **60**:1 (1993), 183–189.

[Freund 1990] L. B. Freund, *Dynamic fracture mechanics*, Cambridge University Press., Cambridge; New York, 1990. 563.

[Geubelle and Kubair 2001] P. H. Geubelle and D. V. Kubair, "Intersonic crack propagation in homogeneous media under shear- dominated loading: numerical analysis", *J. Mech. Phys. Solids* **49**:3 (2001), 571–587.

[Goldshte 1967] R. Goldshte, "On surface waves in joined elastic materials and their relation to crack propagation along junction", *J. Appl. Math. Mech.-Ussr* **31**:3 (1967), 496–502.

[Hutchinson and Suo 1992] J. W. Hutchinson and Z. Suo, "Mixed-mode cracking in layered materials", *Adv. Appl. Mech.* **29** (1992), 63–191.

[Hutchinson et al. 1987] J. W. Hutchinson, M. E. Mear, and J. R. Rice, "On crack paths", *J. Appl. Mech. (Trans. ASME)* **54** (1987), 828–832.

[Kitey and Tippur 2005] R. Kitey and H. V. Tippur, "Dynamic crack growth in particulate bimaterials having discrete and diffuse interfaces: Role of microstructure", *Eng. Fract. Mech.* **72**:18 (2005), 2721–2743.

[Lambros and Rosakis 1995] J. Lambros and A. J. Rosakis, "Shear dominated transonic interfacial crack-growth in a bimaterial. 1. experimental-observations", *J. Mech. Phys. Solids* **43**:2 (1995), 169–188.

[Liu et al. 1993] C. Liu, J. Lambros, and A. J. Rosakis, "Highly transient elastodynamic crack-growth in a bimaterial interface - higher-order asymptotic analysis and optical experiments", *J. Mech. Phys. Solids* **41**:12 (1993), 1887–1954.

[Qian and Sun 1998] W. Qian and C. T. Sun, "A frictional interfacial crack under combined shear and compression", *Compos. Sci. Technol.* **58**:11 (1998), 1753–1761.

[Rosakis et al. 1998] A. J. Rosakis et al., "Intersonic crack propagation in bimaterial systems", *J. Mech. Phys. Solids* **46**:10 (1998), 1789–1813.

[Rosakis et al. 2006] A. J. Rosakis, H. Kanamori, and K. Xia, "Laboratory earthquakes", *Int. J. Fract.* **138**:1–4 (2006), 211–218.

[Sanford and Dally 1979] R. J. Sanford and J. W. Dally, "General-method for determining mixed-mode stress intensity factors from isochromatic fringe patterns", *Eng. Fract. Mech.* **11**:4 (1979), 621–633.

[Singh and Shukla 1995] R. P. Singh and A. Shukla, "Dynamic failure of bimaterial interfaces: A photoelastic investigation", in *Proc. of SEM Spring Conference*, 1995. Grand Rapids, MI: SEM. Available on CD.

[Sun and Qian 1997] C. T. Sun and W. Qian, "The use of finite extension strain energy release rates in fracture of interfacial cracks", *Int. J. Solids Struct.* **34**:20 (1997), 2595–2609.

[Tippur and Rosakis 1991] H. V. Tippur and A. J. Rosakis, "Quasi-static and dynamic crack-growth along bimaterial interfaces - a note on crack-tip field-measurements using coherent gradient sensing", *Exp. Mech.* **31**:3 (1991), 243–251.

[Weertman 1980] J. Weertman, "Unstable slippage across a fault that separates elastic media of different elastic-constants", *J. Geophys. Res.* **85**:NB3 (1980), 1455–1461.

[Xia et al. 2004] K. W. Xia, A. J. Rosakis, and H. Kanamori, "Laboratory earthquakes: The sub-Rayleigh-to-supershear rupture transition", *Science* **303**:5665 (2004), 1859–1861.

[Xia et al. 2005a] K. Xia, A. J. Rosakis, and H. Kanamori, "Supershear and subRayleigh to supershear transition observed in laboratory earthquake experiments", *Exp. Tech.* **29**:3 (2005), 63–66.

[Xia et al. 2005b] K. W. Xia, A. J. Rosakis, H. Kanamori, and J. R. Rice, "Laboratory earthquakes along inhomogeneous faults: Directionality and supershear", *Science* **308**:5722 (2005), 681–684.

[Xia et al. 2006] K. Xia, V. B. Chalivendra, and A. J. Rosakis, "Observing ideal 'self-similar' crack growth in experiments", *Eng. Fract. Mech.* **73** (2006), 2748–2755.

[Yang et al. 1991] W. Yang, Z. Suo, and C. F. Shih, "Mechanics of dynamic debonding", *P. Roy. Soc. Lond. A Mat.* **433**:1889 (1991), 679–697.

Received 8 Apr 2007. Revised 19 Jul 2007. Accepted 23 Jul 2007.

KAIWEN XIA: kaiwen@ecf.utoronto.ca
Department of Civil Engineering, University of Toronto, 35 St. George Street, Toronto ON M5S 1A4, Canada

CARL-ERNST ROUSSEAU: roussea@egr.uri.edu
222-B Wales Hall, Dept. of Mechanical Engineering, University of Rhode Island, Kingston, RI 02881, United States

ARES ROSAKIS: rosakis@aero.caltech.edu
Graduate Aeronautical Laboratory, California Institute of Technology, Pasadena, CA 91125, United States